https://doi.org/10.22226/2410-3535-2021-4-503-507 PACS: 61

Characterization of fragmented structure developed during necking of iron tensile specimen

N. Yu. Zolotorevsky†,1, E. A. Ushanova1,2, V. V. Rybin1, V. N. Perevezentsev3

†zolotorevsky@phmf.spbstu.ru

1Institute of Physics and Mechanics, Peter the Great Polytechnic University, Saint Petersburg, 195251, Russia
2Central Research Institute of Structural Materials "Prometey", Saint Petersburg, 191015, Russia
3Mechanical Engineering Research Institute of the RAS — Branch of Federal Research Center "Institute of Applied Physics of the RAS", Nizhny Novgorod, 603024, Russia

The microstructure fragmentation during necking of the iron tensile specimen was investigated by the electron backscatter diffraction technique. The material under study was the commercially pure iron containing particles of manganese sulfides and oxides. The undeformed mean grain size was ≈54 μm. The aim of the research was the characterization of the structural state preceding ductile rupture. The deformation microstructure was examined on the longitudinal section of the specimen in the locations corresponding to various true strains from ≈1 up to 1.8, which allowed studying the structure evolution in a single specimen. Special attention was paid to the deformation-induced high-angle boundaries, which are known to be preferable sites of microcracks nucleation. It was shown that a considerable number of high-angle boundaries appear already at a strain of ≈1, and their fraction rises with further straining. Large-scale fragmentation peculiarities of different kinds associated with the formation of high angle boundaries were found and discussed in terms of the effect of the neighborhood of grains on their fragmentation. Besides, multiple shear microbands of submicron width inclined to the tensile direction by angles ≈35° and larger were observed in the longitudinal section, which intersect the previously formed deformation substructure. The boundaries of these microbands were shown to make significant contribution to the accumulation of high angle boundaries.

Keywords: metals, deformation, ductile rupture, microstructure, fragmentation.

УДК: 548.4

Изучение фрагментированной структуры, образующейся в шейке при растяжении образца железа

Золоторевский Н. Ю.†,1, Ушанова Э. А.1,2, Рыбин В. В.1, Перевезенцев В. Н.3

1Физико-механический институт, Политехнический университет Петра Великого, Санкт-Петербург, 195251, Россия
2Центральный научно-исследовательский институт конструкционных материалов «Прометей», Санкт-Петербург, 191015, Россия
3Институт машиноведения РАН — филиал Федерального научного центра «Институт прикладной физики Российской академии наук», Нижний Новгород, 6033024, Россия

Методом дифракции обратно рассеянных электронов изучали фрагментированную структуру, которая формируется в шейке образца железа, деформируемого растяжением. Исследуемый материал представлял собой технически чистое железо со включениями сульфидов и оксидов марганца. В исходном состоянии средний размер зерна составлял ≈54 мкм. Целью работы была аттестация структурного состояния, предшествующего вязкому разрушению. На продольном сечении образца исследовали деформационную структуру областей, соответствующих различным степеням истинной деформации, от ≈1 до 1.8, тем самым на одном образце изучали эволюцию структуры. Внимание было сосредоточено на большеугловых границах деформационного происхождения, которые, как ранее было показано, служат местами преимущественного зарождения микротрещин. Показано, что значительное количество большеугловых границ возникает в шейке уже при деформациях ≈1, и их доля увеличивается с ростом степени деформации. Выявлены крупномасштабные особенности деформационной структуры, связанные с образованием большеугловых границ. Их характеристики обсуждаются с точки зрения влияния локального окружения зерна

на его фрагментацию. Кроме того, в продольном сечении образца наблюдаются микрополосы сдвига, составляющие с направлением растяжения углы ≈35° и более, пересекающие ранее образовавшуюся деформационную субструктуру. Границы этих микрополос также дают значительный вклад в накопление большеугловых границ.

Ключевые слова: металлы, деформация, вязкое разрушение, микроструктура, фрагментация.

1. Introduction

The phenomenon of grains fragmentation occurring at large plastic strains has been the subject of many studies in recent decades [1–5]. The main incentive was the creation of ultrafine-grained materials [6]. At the same time, knowledge of laws governing fragmentation is also of interest for studying the physical mechanism of ductile rupture, given that the latter occurs after rather large strains. Early studies carried out using transmission electron microscopy (TEM), showed that voids (microcracks) nucleate in pure metals at deformation-induced boundaries (DIBs) [7–8], predominantly at deformation-induced high-angle boundaries (HABs) [1,7]. Recent studies on tantalum have confirmed that incipient voids were formed not at initial grain boundaries, but at DIBs, and in the overwhelming majority at HABs [9]. The first voids have been detected at true strains of ≈1, which corresponds to approximately half of the maximum local strain reached as a result of necking of tensile specimen [1,9–10]. Therefore, the formation of deformation induced HABs is of particular interest in the context of ductile rupture.

In the present article, polycrystalline iron loaded by tension was under consideration. As far as we know, the structure development during necking in iron has not been investigated systematically before. Some useful information can be provided by the studies of metals subjected to drawing [11,12], since an axisymmetric plastic flow occurs in the central part of the necked gauge region of the tensile specimen. Nevertheless, the data obtained are very limited due to excessively high locality of TEM used in those works. The aim of the current study is to establish main patterns of HABs formation by help of electron backscatter diffraction (EBSD).

2. Experimental

The material under study was 99.9% commercially pure iron containing particles of manganese sulfides and oxides. The undeformed mean grain size was ≈54 μm. Fig. 1a shows one-half of the specimen obtained after failure. It was cut along the tensile direction, and further the longitudinal section was studied. The part of this section adjacent to the fracture surface is represented schematically in Fig. 1b, where also the regions examined by EBSD are depicted. The axes of the specimen (Fig. 1b) are defined as the tensile direction (TD), radial direction (RD) and normal direction (ND).

Local true strains in the neck of specimen were calculated from the local diameters D of the specimen using the equation $\varepsilon = 2\log(D_0/D)$, where $D_0 = 6.15$ mm is the initial diameter of the gauge region of the specimen, thereby assuming that the local strain near the specimen axis is equal to the average strain of the given section as the first approximation. Thus, the estimated local strains in the examined regions are 0.95, 1.15, 1.55 and 1.8. These regions will be referred to as A095, A115, A155 and A180 below.

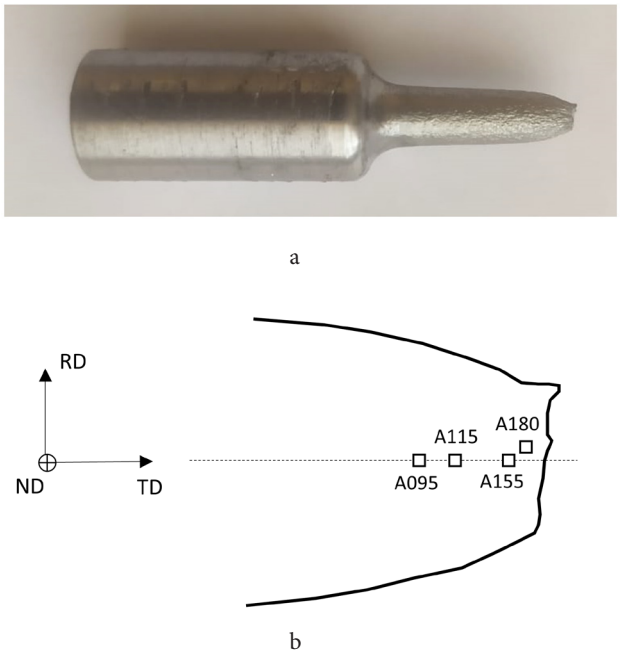

Fig. 1. Tensile specimen (a) and schematic drawing of its longitudinal section with four examined regions indicated (b).

EBSD mapping was carried out with a LYRA 3 XMN RL SEM. The analysis of the orientation maps was performed with a help of the MTEX software [13]. The percentage of non-indexed points in EBSD data presented below was about 20% that enabled sufficiently reliable reconstruction of the (sub)grain structure. At the same time, one should take into account that the procedure of grain reconstruction can create artefacts in cases when, with approaching the place of rupture, large-scale clouds of non-indexed points appear that are probably large voids.

EBSD maps represented in what follows are the inverse pole figure (IPF) maps constructed for TD. Besides, boundaries having misorientations higher than 2° were superimposed on the maps. The color-coding of the boundaries: $2° < \theta < 15°$, light grey; $15° < \theta < 45°$, dark grey; $\theta > 45°$, black. The majority of the regions was scanned using a stepsize of 200 nm, while some smaller areas were examined with a stepsize of 50 nm. In order to estimate the fraction of deformation-induced HABs, the earlier proposed method has been used allowing separation of the contributions from DIBs. It included the following steps: (i) determination of the misorientation distribution of all boundaries in terms of length fraction, $L_{all}(\theta)$, (ii) separation of original grain boundaries and determination of their contribution, $L_{OGB}(\theta)$, to the overall misorientation distribution, (iii) obtaining finally the misorientation distribution of DIBs, $L_{DIB}(\theta)$, by subtracting $L_{OGB}(\theta)$ from $L_{all}(\theta)$. This procedure was described in detail in Ref. [14].

3. Results

Fig. 2 shows the percentage of deformation-induced HABs among other DIBs as a function of the local strain. One can see that a considerable amount of HABs (≈8%) appears already at a strain of 0.95, and their fraction rises with strain. In addition, the results obtained earlier for iron deformed by compression [15] are represented here. As can be seen, the fraction of HABs formed in tension is a little more than in compression. This may be associated with a difference in the patterns of structure evolution, however it seems premature to draw conclusions, in particular, because actual strain at the specimen axis may be some larger than the strain averaged over cross-section [16].

Let us consider now what patterns of structural evolution are behind these percentages of deformation-induced HABs.

Fig. 3a shows the microstructure of region A095 together with the inverse pole figures, which represent the microtexture of the areas marked on the orientation map by dashed contours. One can see the appearance of considerable orientation non-uniformity of original grains associated with the developing deformation substructure. It is well known that dislocation cells first appear separated by walls in which dislocations are concentrated, and only later the fragment boundaries stand up against the cell structure because of higher misorientations and more dense constitution [1,4]. Fig. 3b shows the map of "band slope" (BS), which is the diffraction pattern characteristic sensible to the local concentration of dislocations, obtained from the area marked on the map of Fig. 3a by the white frame. The substructure composed of submicron cells occurs here. The misorientations between most cells are lower than 2°. Nevertheless, accumulation of small rotations over a large distance across the grain results in the grain-scaled orientation gradients, which can be observed on the orientation map.

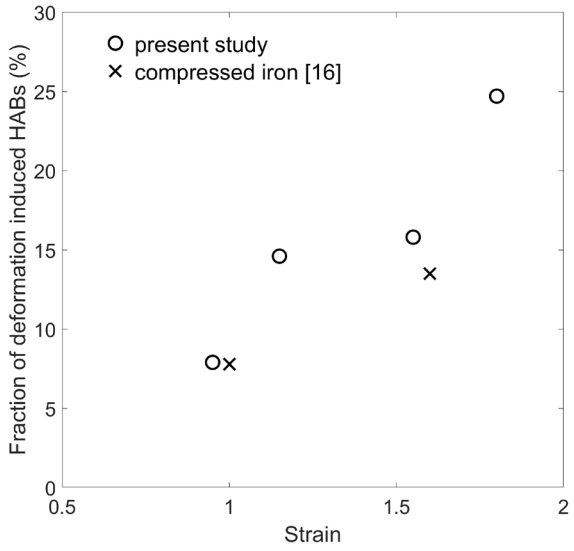

Fig. 2. Percentage of deformation-induced HABs as a function of local strain in the gauge regions of specimen. The results for compressed iron [16] are also presented.

At some DIBs, the misorientation increases to the point that it exceeds a critical angle (15° is commonly accepted), at which dislocation subboundaries transform to the boundaries of intergranular type. Such high-angle portions of DIBs are most frequent in the vicinity of grain boundaries, that is natural given the role of the latter at an early stage of fragmentation [1]. At the same time, large-scale peculiarities of fragmentation, which seems to be the main contributors to the HAB production, attract attention.

Peculiarities of the first kind can be seen in region A095; two such features are indicated in Fig. 3a by white arrows. These are extended boundaries elongated parallel to the tensile axis. They can be distinguished from original grain boundaries, in particular, by the alternation of low and high angle segments. Besides, their morphology is more complicated: the upper one is a zone of intense fragmentation rather than a distinct boundary.

Structural peculiarities of the second kind are large closed fragments with a cross size of ≈10 mm or larger. One can see them both in region A095 (Fig. 3a) and region A115 (Fig. 4). Unlike boundaries of the first kind, their boundaries are rather uniform, with misorientation varying along the boundary only slightly. It should be emphasized that, at this stage of deformation, such fragments are always adjacent to original grain boundaries.

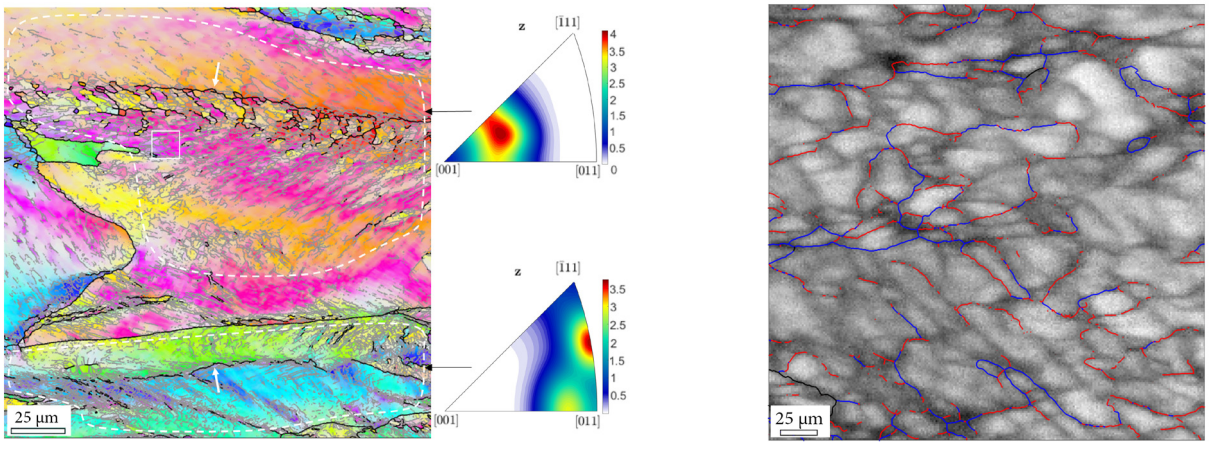

a b

Fig. 3. (Color online) Region A095: EBSD map together with TD inverse pole figures of areas marked by dashed contours on the map (a), and BS map of the area marked by white frame on the panoramic map (b). On the BS map, the boundaries with $\theta > 2°$ are drawn: $2° < \theta < 5°$ (red), $\theta > 5°$ (blue).

Fig. 4 also presents peculiarities of the third kind, namely the widely spaced microbands of about 1 μm in width inclined to TD in the longitudinal section by angles from ≈35° to 45°, which intersect previously formed deformation substructure. It may be seen that the crystal lattice within different microbands was rotated relative to the matrix in the same direction albeit to varying degrees, up to ≈45°. The area marked by white frame on the map of Fig. 4 has been scanned with a stepsize of 50 nm (Fig. 5). One can see in Fig. 5 a that, in addition to micron width bands detected on the map of Fig. 4, much narrower bands occur having the width down to ≈0.1 μm. The misorientation angles at their boundaries vary from ≈20° to 40° (Fig. 5 b). Hence, if such a small step had been used for the whole region A115, a fraction of deformation-induced HABs would be even greater than the value presented in the graph of Fig. 2.

These microbands are similar to the bands observed in an aluminium alloy [5] and IF steel [17] after cold rolling. It was shown in those studies that these are the bands of the localized shear, referred to as "microshear bands" [5] or "S-bands" [17]. Given the similarity between the patterns of banding, one can suppose that such bands occur in our case as well. Note that two grains, in which microbands occur, have substantially different orientations (Fig. 4). Thus, our examination does not show apparent orientation dependence of the microbanding.

When the examined region approaches the fracture surface, the degree of fragmentation rises owing to increasing local strain. Correspondently, the boundaries having various features described above can be found in regions A155 (Fig. S1, Supplementary material) and A180 (Fig. S2, Supplementary material), though it is not always easy to discriminated DIBs of the first two kinds due to general refinement and complication of the structure. At the same time, it should be noted that non-fragmented areas with rather uniform orientation remain even at so large strains.

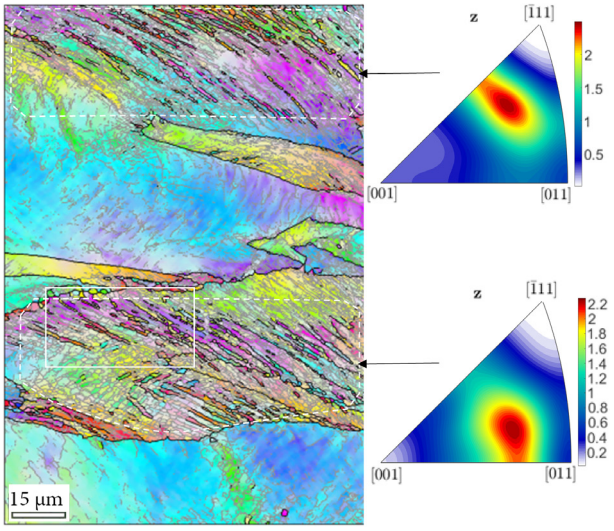

Fig. 4. (Color online) EBSD map of region A115 together with TD inverse pole figures of areas marked on the map by dashed contours.

4. Discussion

It is known that large-scale fragmentation is closely related to the grain-to-grain plastic interaction [1,18,19]. Particularly this interaction is meaningful in bcc metals deformed by uniaxial extension. In the case of cold drawing, the grains, which have orientations close to the stable <110>, undergo plane deformation accompanied by bending rather than axisymmetric deformation corresponding to the macroscopic shape change [11,20]. Other grains have to accommodate themselves to this non-uniform deformation. As a result, they become strongly fragmented while their considerable parts retain orientations strongly deviated from <110> even at large strains [21]. The inverse pole figures presented in Figs 3 and 4 as well as other microtextures recorded in the present study show that similar microtexture evolution seems to occur in the neck of iron specimen, namely, grain orientations are scattered throughout the standard stereographic triangle.

Therefore, it would be reasonable to consider peculiarities of fragmentation described in the previous section in terms of the effect of grain neighborhood. Suppose, for example, that a difference in slip system combinations operating in two half-fractions of a grain appears under the influence of its neighborhood. Either of the two regions contacts with more than one adjacent grains and has to conform to their deformation. Hence, the patterns of the slip operating in these regions will most probably be non-uniform. One may expect in such a case that a deformation-induced boundary having a

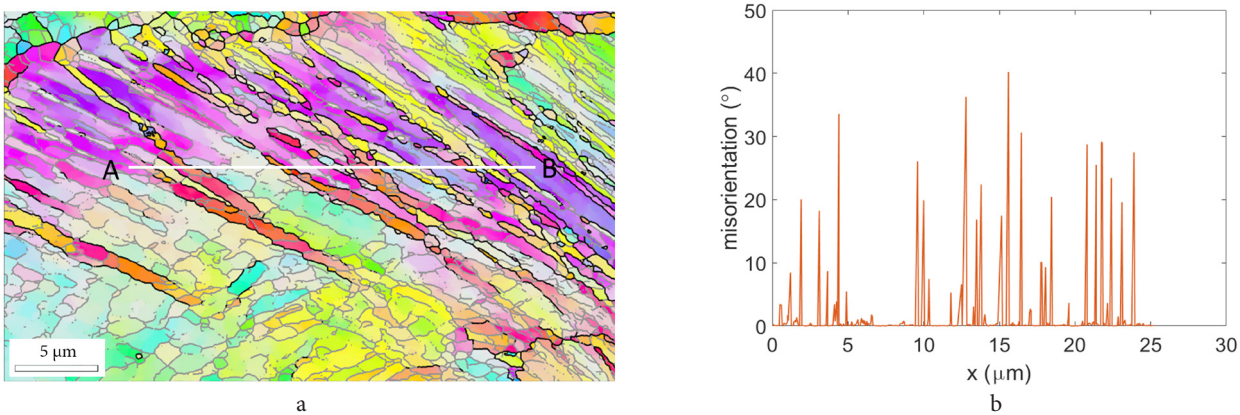

a b

Fig. 5. (Color online) Refined map of the area marked by white frame on the panoramic map of Fig. 4 (a), and point-to-point misorientation distribution along the segment AB (b).

significantly non-uniform misorientation will be formed or, alternatively, a transition zone instead a simple boundary will develop. Those are just the characteristics of the structural peculiarities of the first kind. On the other hand, if a part of the initial grain, in which a slip pattern changes, has smaller size and contacts with only one adjacent grain, a combination of active slip systems in it may by quite uniform. In such a case, a fragment would appear having rather perfect boundary, just as it was observed for the structural peculiarities of the second kind.

As for shear microbands, which seem to be the most effective suppliers of HABs, their formation may be controlled by the intrinsic laws of grain structure evolution rather than by the effect of neighborhood. Although the origin of the microbands remains unclear [5,17], it is likely that they originate from an instability of previously formed substructure due to the change of grain orientation during straining, similar to those developing at a strain-path change [22]. In the case of cold rolling, the shear microbands appear at strains ≈0.5, and misorientations at their boundaries are initially low [5,17]. Further development of the microbands with increasing strain results in progressive reorientation of material within them, which, in its turn, may result in the formation of HABs. The latter must rotate with straining in accordance with a rigid body rotation (example of such a development one can presumably see in Fig. S2 a, Supplementary material), so that at large strains ≈2 they become aligned parallel to the tensile direction [5,17] and indistinguishable from other HABs.

5. Conclusion

In this research, peculiarities of the microstructure fragmentation in the neck of iron tensile specimen were investigated. Special attention was paid to deformation-induced HABs, which are preferable sites of microcrack origination. The following main conclusions were drawn.

1. The researcher can study the fragmentation evolution with increasing strain on a sinle sample by examining the microstructure formed in different regions of the neck.

2. Peculiarities of large-scale fragmentation of different kinds providing new HABs occur, the features of which are governed greatly by the effect of grain neighborhood.

3. The boundaries of the shear microbands make the largest contribution to the total fraction of HABs.

Supplementary material. *The online version of this paper contains supplementary material available free of charge at the journal's Web site (lettersonmaterials.com).*

Acknowledgements. The Russian Science Foundation supported this work, project No. 21-19-00366.

References

1. V. V. Rybin. Large plastic deformations and fracture of metals. Metallurgiya, Moscow (1986) 224 p. (in Russian) [В. В. Рыбин. Большие пластические деформации и разрушение металлов. Металлургия, Москва (1986) 224 с.]
2. V. V. Rybin, A. A. Zisman, N. Y. Zolotorevsky. Acta Metall. Mater. 41, 2211 (1993). Crossref
3. D. A. Hughes, N. Hansen. Acta Mater. 45, 3871 (1997). Crossref
4. N. Hansen, D. Juul Jensen. Materials Science and Technology. 27, 1229 (2011). Crossref
5. P. J. Hurley, F. J. Humphreys. Acta Mater. 51, 1087 (2003). Crossref
6. T. G. Langdon. Acta Mater. 61, 7035 (2013). Crossref
7. V. V. Rybin, V. A. Likhachev, A. N. Vergazov. Fizika Metallov i Metalloved. 37, 620 (1974). (in Russian) [В. В. Рыбин, В. А. Лихачев, А. Н. Вергазов. ФММ. 37, 620 (1974).]
8. R. N. Gardner, T. C. Pollock, H. Wilsdorf. Mater. Sci. Eng. 29 (2), 169 (1977). Crossref
9. P. Noell, J. Carroll, K. Hattar, B. Clark, B. Boyce. Acta Materialia. 137, 103 (2017). Crossref
10. M. S. Milza, D. C. Barton, P. Church, J. L. Sturges. J. Phys. IV France. 7 (C3), 891 (1997). Crossref
11. G. Landford, M. Cohen. Metall. Trans. A. 6, 901 (1975). Crossref
12. E. V. Nesterova, V. V. Rybin, N. Yu. Zolotorevsky. The Physics of Metals and Metallography. 89, 42 (2000).
13. R. Hielscher, F. Bachmann, D. Mainprice, R. Kilian. MTEX 5.2.8 (2020). Website
14. N. Yu. Zolotorevsky, V. V. Rybin, A. N. Matvienko, E. A. Ushanova, S. A. Philippov. Materials Characterization. 147, 184 (2019). Crossref
15. N. Yu. Zolotorevsky, V. V. Rybin, A. N. Matvienko, E. A. Ushanova, S. N. Sergeev. Letters on Materials. 8 (3), 305 (2018). Crossref
16. M. Kuroda, A. Uenishi, H. Yoshida, A. Igarashi. International Journal of Solids and Structures. 43, 4465 (2006). Crossref
17. B. L. Li, A. Godfey, Q. M. Meng, Q. Liu, N. Hansen. Acta Mater. 52, 1069 (2004). Crossref
18. A. K. Kanjarla, L. Delannay, P. Van Houtte. Metall. Mater. Trans. A. 42, 660 (2011). Crossref
19. A. Zisman. Int. J. Eng. Sci. 116, 155 (2017). Crossref
20. W. F. Hosford Jr. Trans. Metall. Soc. AIME. 230, 12 (1964).
21. N. Yu. Zolotorevskii, E. V. Nesterova, V. V. Rybin, Yu. F. Titovets. The Physics of Metals and Metallography. 99 (1), 73 (2005).
22. A. Zisman, E. Nesterova, V. Rybin, C. Teodosiu. Scripta Materialia. 46, 729 (2002). Crossref